International Journal of Solids and Structures 46 (2009) 4504–4514

Contents lists available at ScienceDirect

International Journal of Solids and Structures

journal homepage: www.elsevier.com/locate/ijsolstr

Two-fold symmetrical 6R foldable frame and its bifurcations

Yan Chen [a], Zhong You [b,*,1]

[a] School of Mechanical and Aerospace Engineering, Nanyang Technological University, 50 Nanyang Avenue, Singapore 639798, Singapore
[b] Department of Engineering Science, University of Oxford, Parks Road, Oxford OX1 3PJ, UK

ARTICLE INFO

Article history:
Received 29 January 2009
Received in revised form 6 July 2009
Available online 17 September 2009

Keywords:
Kinematics
Deployable structures
Mechanisms
Bricard linkage
Bifurcation

ABSTRACT

In this paper, we have discovered that a type of two-fold symmetrical 6R foldable frame proposed as a deployable core structure to support solar blankets in space applications is actually a line and plane-symmetric Bricard linkage. Using the singular value decomposition of the Jacobian matrix of closure equations, we are able to show that bifurcations exist during deployment of the frame. And the bifurcations cannot be avoided in current designs. However, we also identified a feasible area for design parameters in which bifurcations can be completely removed. A physical model has been made which proves that our conclusion is correct.

1. Introduction

Deployable polygonal frames are widely used in aerospace structures to support antenna reflectors and solar blankets (Fang et al., 2004). First proposed by Crawford et al. (1973), the frames consist of a closed loop of bars connected by revolute hinges. They can have various forms, from squares, rectangles to hexagons. A comprehensive review of its applications was given by Gan and Pellegrino (2006).

This paper focuses on rectangular frames. A conceptual design of such frames was proposed by Pellegrino et al. (2000) and Hutt (2007). The frame, shown in Fig. 2, consists of a loop of 6 links of square cross sections connected by revolute hinges. The frame has two-fold symmetry. It expands to a rectangular profile and can be packaged into a bundle. Two side bars, 2 and 3 and 5 and 6, remain parallel in its conventional deployment, which makes it ideal as a support frame for solar blankets because it can be rolled onto the parallel bars. However, it has been noted that there exists bifurcation during deployment.

In this paper, using the technique employed by us previously for 4*R* frames (Chen and You, 2006), we shall show that the foldable 6*R* rectangular frame is in fact an alternative form of a special kind of Bricard linkage with both line and plane symmetry (Bricard, 1897, 1927). Comprehensive reviews on the Bricard linkage and relevant 6*R* overconstrained linkages can be found in Baker (1980), Phillips (1990), Chen (2003) and Cui and Dai (2009). Because of the symmetric characteristics, this special Bricard linkage has bifurcations during deployment. By a comprehensive analysis of the kinematic characters of this special Bricard linkage using the technique similar to that proposed by Gan and Pellegrino (2006), we are able to detect these bifurcations. Moreover, we have found a feasible set of design parameters that lead to construction of frames without bifurcation. This discovery removes the requirement of additional appendages to avoid deployment bifurcations and therefore greatly improves the deployment reliability of the frame.

The layout of the paper is as follows. Section 2 establishes a link between the special Bricard linkage and the foldable 6*R* frame. In Section 3, a kinematic analysis is conducted in order to investigate the bifurcations. Based on the analysis, a new frame design without motion bifurcation is presented in Section 4. Conclusions and further discussion is given in Section 5 which ends the paper.

2. The special case of Bricard linkage and the foldable six-bar frame

2.1. The Bricard linkages

The Bricard 6R linkages have six distinct types, that can be summarised as follows (Baker, 1980; Phillips, 1990).

(a) The general line-symmetric case

$$\begin{aligned} &a_{12}=a_{45}, \quad a_{23}=a_{56}, \quad a_{34}=a_{61} \\ &\alpha_{12}=\alpha_{45}, \quad \alpha_{23}=\alpha_{56}, \quad \alpha_{34}=\alpha_{61} \\ &R_1=R_4, \quad R_2=R_5, \quad R_3=R_6 \end{aligned} \tag{1}$$

* Corresponding author.
E-mail address: zhong.you@eng.ox.ac.uk (Z. You).
[1] During the preparation of this paper, Haitian visiting scholar, Department of Engineering Mechanics, Dalian University of Technology, 116024 Dalian, China.

0020-7683/$ - see front matter © 2009 Elsevier Ltd. All rights reserved.
doi:10.1016/j.ijsolstr.2009.09.012

Notations

C	Cosine
S	Sine
$[I]$	Unit matrix
l_1, l_2	Actual side length of the 6R frame
R	Offset of links of a Bricard linkage
R_i	Distance from link $(i-1)i$ to link $i(i+1)$ positively about Z_i. Also referred as the *offset* of joint i
$[T_{i(i+1)}]$	Transfer matrix between system of link $(i-1)i$ and system of link $i(i+1)$
X_i	Axis commonly normal to Z_{i-1} and Z_i, positively from joint $i-1$ to joint i
Z_i	Axis of hinge (revolute joint) i
a	Length of links of a Bricard linkage
$a_{i(i+1)}$	Distance between axes Z_i and Z_{i+1}. Also referred as the *length* of link $i(i+1)$
α	Twist of links of a Bricard linkage
$\alpha_{i(i+1)}$	Angle of rotation angle from axes Z_i to Z_{i+1} positively about axis X_i. Also referred to as the *twist* of link $i(i+1)$
μ	Geometric parameter
θ_i^d	Revolute variable of a linkage when the alternative form of the linkage is in its fully deployed configuration
θ_i^f	Revolute variable of a linkage when the alternative form of the linkage is in its fully folded configuration
θ_i	Revolute variable of the linkage, which is the angle of rotation from X_{i-1} to X_i positively about Z_i
θ_i^b	Revolute variable of the linkage at bifurcationThe coordinate systems, geometrical parameters and variables related to the revolute connected links are shown in Fig. 1.

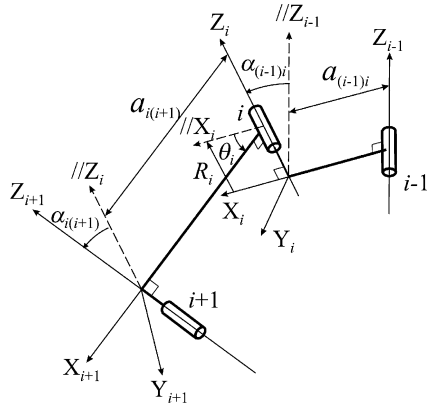

Fig. 1. Coordinate systems, parameters and variables for two adjacent links connected by revolute joints.

(b) The general plane-symmetric case

$$\begin{aligned} &a_{12}=a_{61},\quad a_{23}=a_{56},\quad a_{34}=a_{45}\\ &\alpha_{12}+\alpha_{61}=2\pi,\quad \alpha_{23}+\alpha_{56}=2\pi,\quad \alpha_{34}+\alpha_{45}=2\pi,\\ &R_1=R_4=0,\quad R_2=-R_6,\quad R_3=-R_5 \end{aligned} \tag{2}$$

(c) The trihedral case

$$\begin{aligned} &a_{12}^2+a_{34}^2+a_{56}^2=a_{23}^2+a_{45}^2+a_{61}^2\\ &\alpha_{12}=\alpha_{34}=\alpha_{56}=\frac{\pi}{2},\quad \alpha_{23}=\alpha_{45}=\alpha_{61}=\frac{3\pi}{2}\\ &R_i=0\ (i=1,2,\ \ldots,6) \end{aligned} \tag{3}$$

(d) The line-symmetric octahedral case

$$\begin{aligned} &a_{12}=a_{23}=a_{34}=a_{45}=a_{56}=a_{61}=0\\ &R_1+R_4=R_2+R_5=R_3+R_6=0 \end{aligned} \tag{4}$$

(e) The plane-symmetric octahedral case

$$\begin{aligned} &a_{12}=a_{23}=a_{34}=a_{45}=a_{56}=a_{61}=0\\ &R_4=-R_1,\ R_2=-R_1\frac{\sin\alpha_{34}}{\sin(\alpha_{12}+\alpha_{34})},\quad R_5=R_1\frac{\sin\alpha_{61}}{\sin(\alpha_{45}+\alpha_{61})},\\ &R_3=R_1\frac{\sin\alpha_{12}}{\sin(\alpha_{12}+\alpha_{34})}\quad\text{and}\quad R_6=-R_1\frac{\sin\alpha_{45}}{\sin(\alpha_{45}+\alpha_{61})} \end{aligned} \tag{5}$$

(f) The doubly collapsible octahedral case

$$\begin{aligned} &a_{12}=a_{23}=a_{34}=a_{45}=a_{56}=a_{61}=0\\ &R_1R_3R_5+R_2R_4R_6=0 \end{aligned} \tag{6}$$

Figs. 3 and 4 show the line-symmetric and plane-symmetric Bricard linkage in motion sequences, respectively. For the first linkage, each joint or link of the linkage is line-reflected in the line of symmetry, which is located in the centre of the linkage, whereas for the second one, they are plane-reflected in the plane of symmetry, which always passes through joint axes 1 and 4.

2.2. The 6R foldable frame

The geometry of the 6R foldable frame proposed by Pellegrino et al. (2000) is shown in Fig. 5. Six bars with square cross section, 1–2, 2–3, 3–4, 4–5, 5–6 and 6–1, are connected by six hinges at 1, 2,

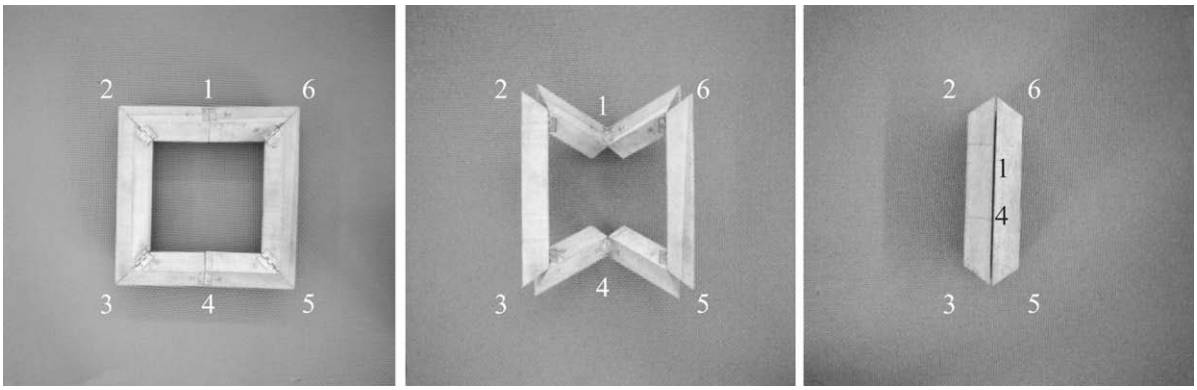

Fig. 2. The folding sequence of the 6R foldable frame.

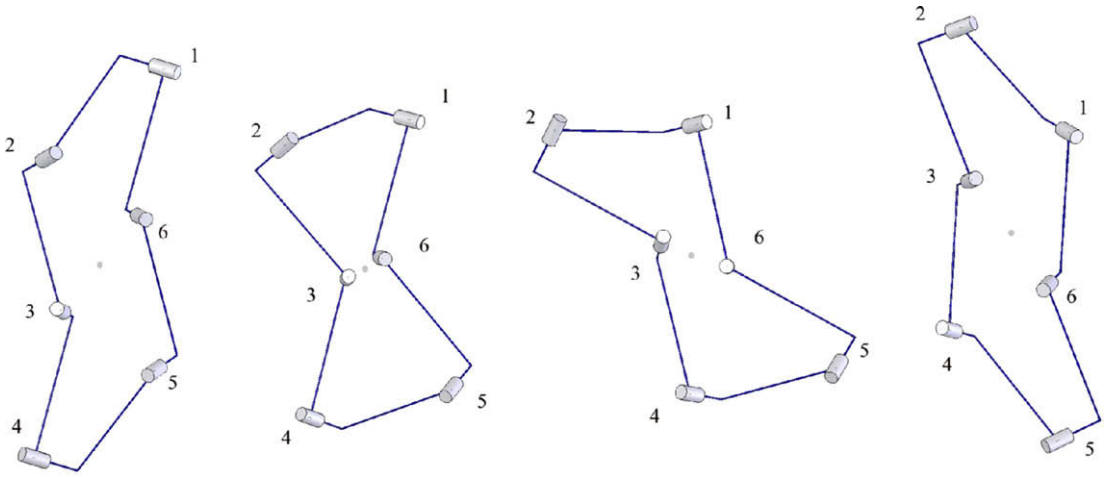

Fig. 3. The motion sequence of a line-symmetric Bricard linkage.

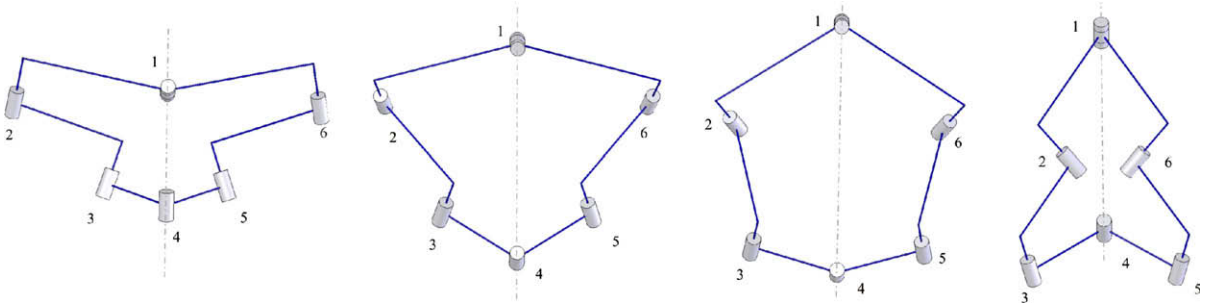

Fig. 4. The motion sequence of a plane-symmetric Bricard linkage.

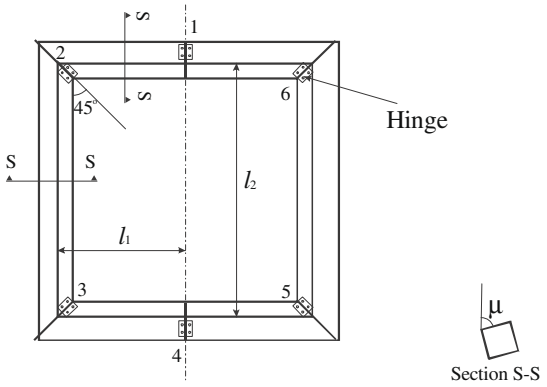

Fig. 5. The geometry of the 6*R* foldable frame.

3, 4, 5 and 6, to form a rectangular frame with a symmetric plane passing through hinges 1 and 4. Note that the bars are laid tilted by an angle μ, and the hinges are placed on either the inner or outer surface of the bars. The frame can be folded into a bundle. Links 12, 34, 45, and 61 have length l_1, and links 23 and 56 have length l_2. The conventional folding sequence of such a frame is shown in Fig. 2. When $2l_1 < l_2$, the frame can be folded and hinges 1 and 4 are a distance apart in the folded configuration. When $2l_1 = l_2$, the frame is a square and hinges 1 and 4 meet when completely folded. When $2l_1 > l_2$, the frame cannot be completely folded as hinges 1 and 4 collide during folding.

This 6*R* frame is a linkage with usually one internal mobility. It is not in the original form of a 6*R* linkage because in mechanism theory, links always span the shortest distance between two adjacent revolute hinges, whereas here the physical links do not. Thus we name the frame as the alternative form of the original linkage. By extending the hinge axes of the six-bar frame, we are able to identify the corresponding links of the original linkage, see Fig. 6.

Because of symmetry of the 6*R* frame, we have

$$a_{12} = a_{34} = a_{45} = a_{61}. \tag{7a}$$

Since axes of joints 2 and 3 meet at point A and axes of joints 5 and 6 meet at point B, we have

$$a_{23} = a_{56} = 0. \tag{7b}$$

Following the convention given by Beggs (1966), we can define axes *X*'s and *Z*'s in the original 6R linkage shown in Fig. 7. Let X_3 at point A be perpendicular to both Z_2 and Z_3 and point out of the paper, and X_6 at point B be perpendicular to axes Z_5 and Z_6 and also point out of the paper, as shown in Fig. 7. So the twists of the linkage are

$$\alpha_{12} = \alpha_{45} = \frac{3\pi}{2}, \quad \alpha_{34} = \alpha_{61} = \frac{\pi}{2}, \tag{8a}$$

$$\alpha_{23} = \alpha_{56}. \tag{8b}$$

and

$$R_1 = R_4 = 0 \quad \text{and} \quad -R_2 = R_3 = -R_5 = R_6. \tag{9}$$

Compare (7)–(9) with (1), we can conclude this original linkage is a line-symmetric Bricard linkage with a symmetric line passing through the centre and perpendicular to the paper for the configuration in Fig. 7.

Note that, if either X_3 or X_6 is reversed, which is possible because they correspond to zero length links, the twists α_{23} or

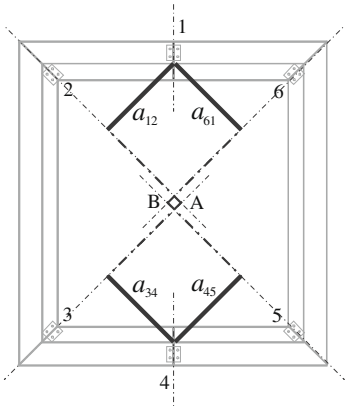

Fig. 6. The 6*R* frame and its original linkage.

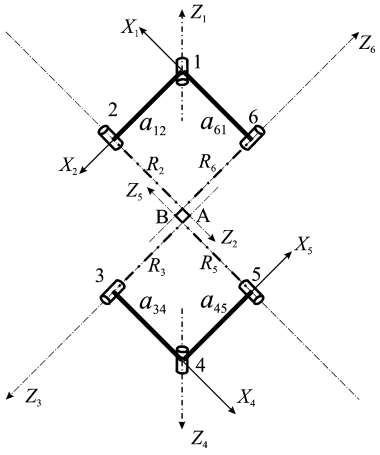

Fig. 7. The original Bricard linkage. Note that axes X_3 and X_6 are not drawn.

α_{56} have to change accordingly. For instance, if X_6 reverses its direction, (8b) becomes

$$\alpha_{56} = 2\pi - \alpha_{23}.$$

which indicates that this original linkage is actually a plane-symmetric Bricard linkage by comparing it with (2).

We therefore conclude that the corresponding original linkage of the 6*R* frame is a special Bricard linkage with *both line and plane symmetries*. Next, we try to find the relationship between the geometric parameters of the original linkage and those of the alternative form.

Because of symmetry, only links 12 and 23 are studied, as shown in Fig. 8 with both the original linkage and the alternative form. Let $\overline{ED} = l_1$ and $\overline{EG} = l_2$. We have

$$\angle DEM = \angle KEM = \arcsin\frac{1}{\sqrt{1+\cos^2\mu}}.$$

DM is the link 12 in original linkage; MA is the offset of joint 2; and $\angle FAH$ is the twist of link 23. So we have

$$a_{12} = \frac{l_1}{\sqrt{1+\cos^2\mu}},$$

$$R_2 = \frac{l_2}{2}\frac{\sqrt{1+\cos^2\mu}}{\cos\mu} - l_1\frac{\cos\mu}{\sqrt{1+\cos^2\mu}} \quad \text{and}$$

$$\alpha_{23} = \arccos\frac{1-\cos^2\mu}{1+\cos^2\mu} \tag{10}$$

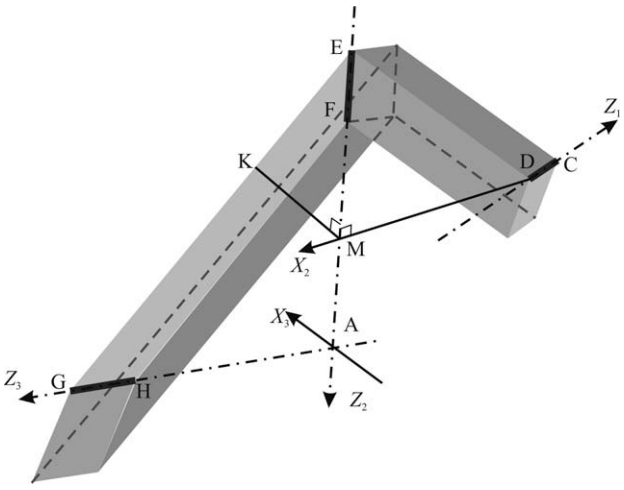

Fig. 8. The detailed links of six-bar frame and its original linkage.

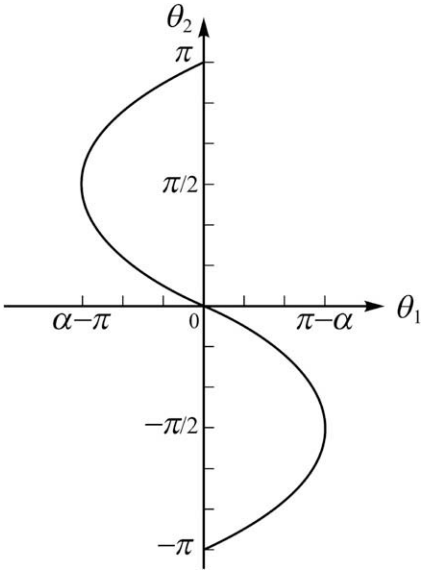

Fig. 9. The general kinematic path for the Bricard linkage.

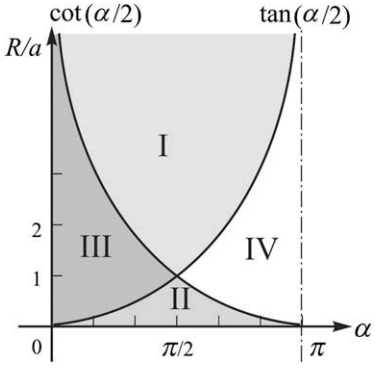

Fig. 10. Four cases in kinematic analysis.

For the 6*R* frame, the kinematic angles of the original linkage corresponding to the fully deployed and fully folded configurations are

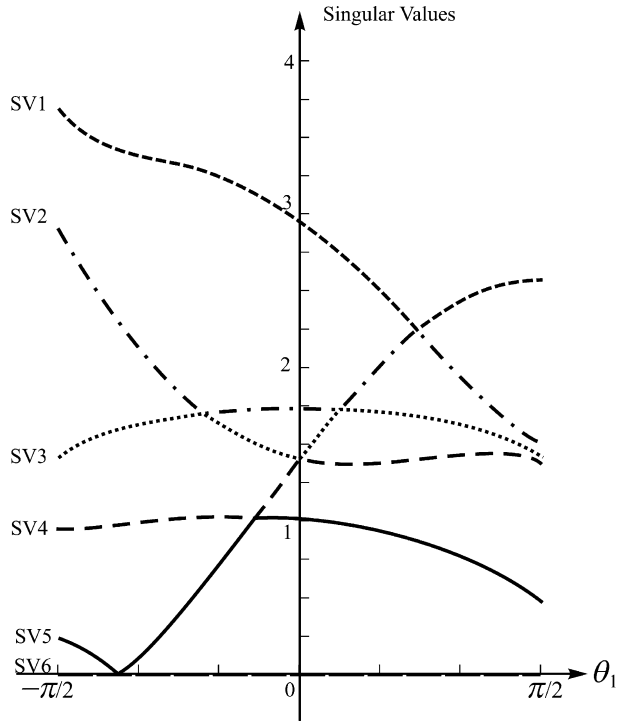

Fig. 11. Singular values of Jacobian matrix vs. θ_1 for a linkage with $R/a = 3/2$ and $\alpha = \pi/2$. The sixth singular value (SV6) is always zero.

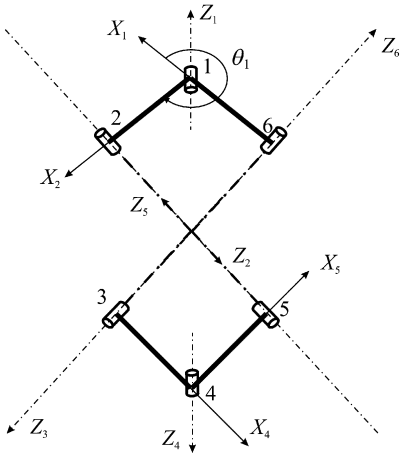

Fig. 12. The linkage at bifurcation configuration.

$$\theta_1^d = 2\arcsin\frac{1}{\sqrt{1+\cos^2\mu}} - \pi,$$
$$\theta_2^d = \frac{\pi}{2} + \arccos(\cos^2\mu),$$
$$\theta_1^f = -2\arcsin\frac{1}{\sqrt{1+\cos^2\mu}} \quad \text{and} \quad \theta_2^f = \frac{3\pi}{2} \tag{11}$$

Superscripts '*d*' and '*f*' indicate the deployed and fully folded configurations.

3. The analysis of kinematic path and bifurcation

For a 6*R* foldable frame, the geometric parameters of the original line and plane-symmetric Bricard linkage can be obtained from (10). The parameters with line-symmetric case in (7)–(9) will be used for derivation of kinematic path. So the closure equation is, using Denavit and Hartenberg notation (Beggs, 1966),

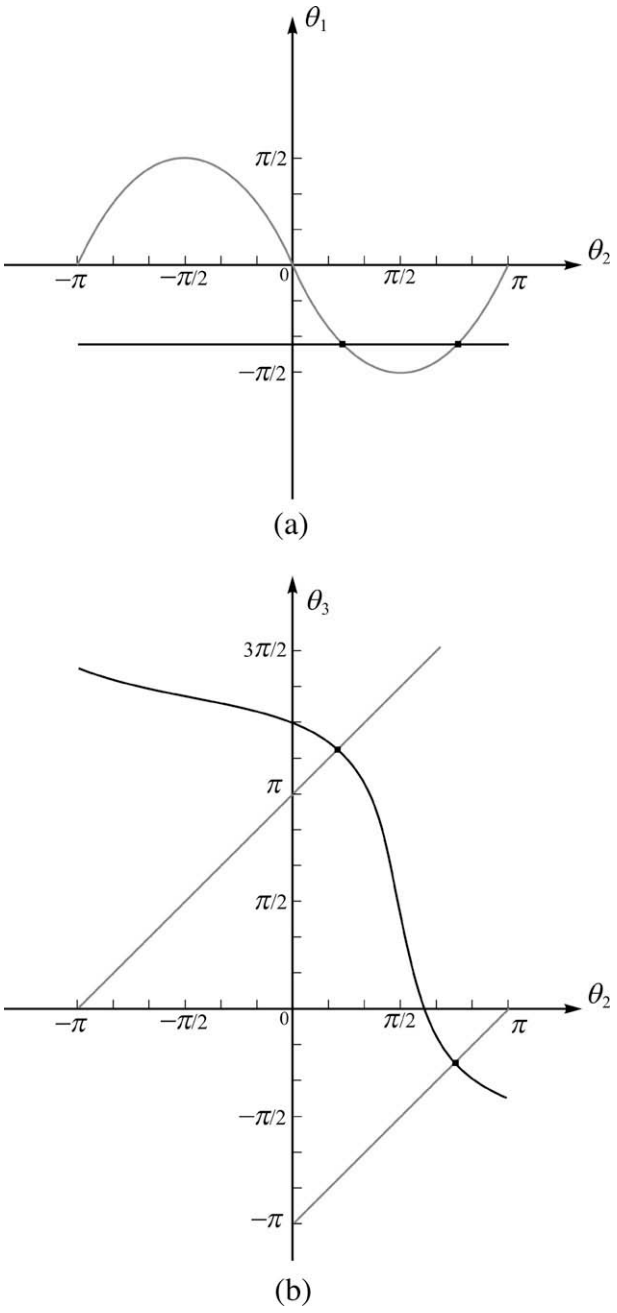

Fig. 13. Kinematic paths of the linkage with $R/a = 3/2$ and $\alpha = \pi/2$, where the path for the line and plane-symmetric Bricard linkage is in grey and the one for 4*R* spherical linkage is in black. The intersection points of two paths in '■' are the bifurcation points. (a) θ_1 vs. θ_2 and (b) θ_3 vs . θ_2.

$$[T_{61}]\cdots[T_{34}][T_{23}][T_{12}] = [I] \tag{12}$$

where

$$[T_{i(i+1)}] = \begin{bmatrix} C\theta_i & S\theta_i & 0 & -a_{i(i+1)} \\ -C\alpha_{i(i+1)}S\theta_i & C\alpha_{i(i+1)}C\theta_i & S\alpha_{i(i+1)} & -R_iS\alpha_{i(i+1)} \\ S\alpha_{i(i+1)}S\theta_i & -S\alpha_{i(i+1)}C\theta_i & C\alpha_{i(i+1)} & -R_iC\alpha_{i(i+1)} \\ 0 & 0 & 0 & 1 \end{bmatrix}, \tag{13}$$

($i = 1, 2, \ldots, 6$ and when i+1>6, it is replaced by 1).

The closure Eq. (12) contains six unknown variables, θ_1–θ_6, and usually only one of them is independent because this linkage has in general one degree of mobility. A numerical method, the singular

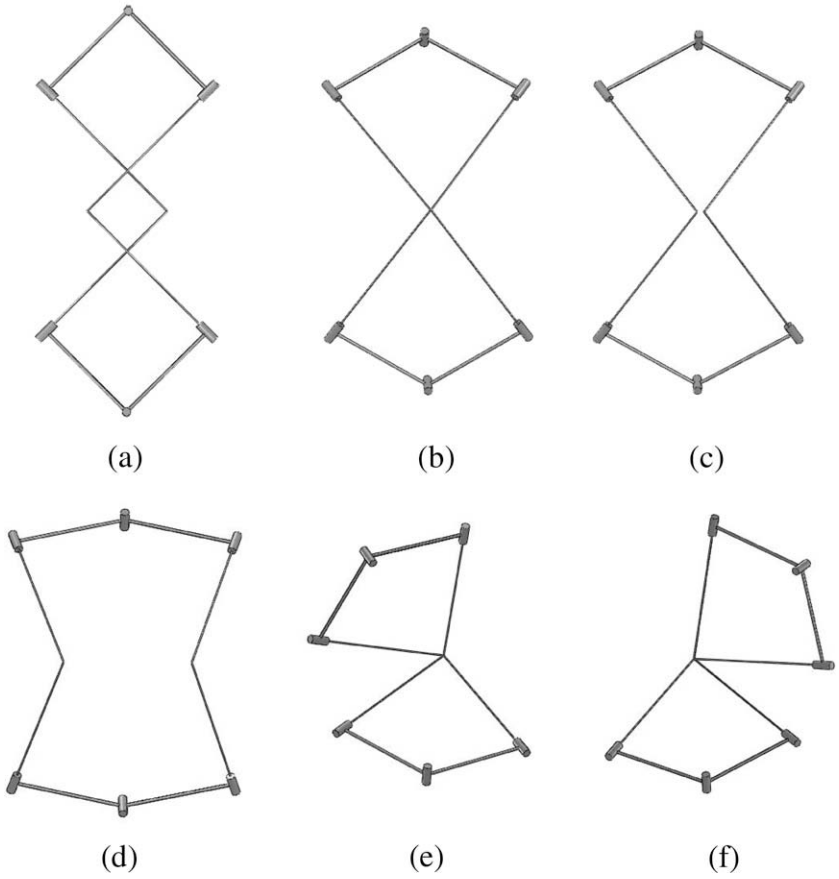

Fig. 14. Motion sequence of the linkage passing the bifurcation point. (a) Configuration with $\theta_1 = -\pi/2$ and $\theta_2 = \pi/2$; (b) bifurcation point; (c) and (d) on the path of line- and plane-symmetric Bricard linkage; (e) and (f) on the path of a spherical 4*R* linkage.

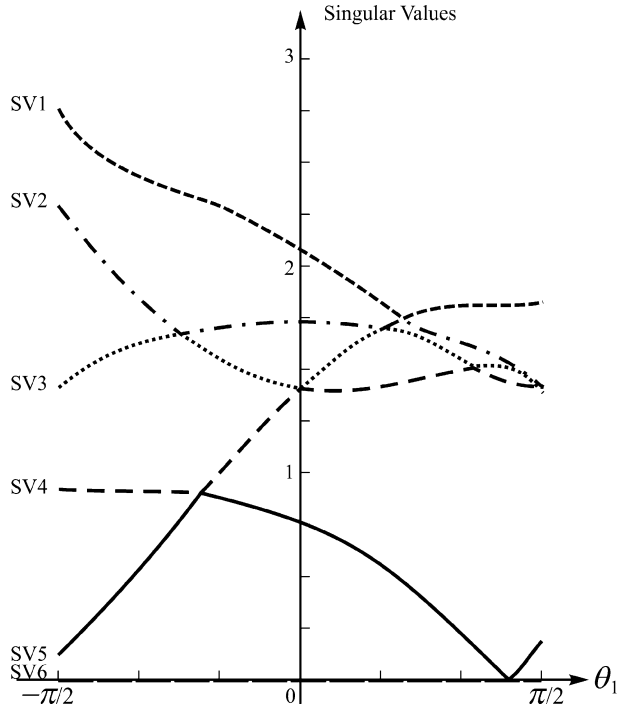

Fig. 15. Singular values of Jacobian matrix vs. θ_1 for a linkage with $R/a = 4/5$ and $\alpha = \pi 2$. The sixth singular value (SV6) is always zero.

value decomposition of Jacobian matrix of the system with the predictor and corrector steps (Lay, 2003; Gan and Pellegrino, 2006), is applied to obtain the kinematic path. The detail of this approach is given in Appendix A.

For the original linkage of the 6*R* frame, we set

$$a_{12} = a_{34} = a_{45} = a_{61} = a, \tag{14a}$$
$$a_{23} = a_{56} = 0, \tag{14b}$$
$$\alpha_{12} = \alpha_{45} = \frac{3\pi}{2}, \quad \alpha_{34} = \alpha_{61} = \frac{\pi}{2}, \tag{14c}$$
$$\alpha_{23} = \alpha_{56} = \alpha, \tag{14d}$$
$$R_1 = R_4 = 0 \tag{14e}$$

and

$$-R_2 = R_3 = -R_5 = R_6 = R. \tag{14f}$$

The general kinematic path of this mechanism is shown in Fig. 9. It is found that the path is independent of *R* and *a*.

In the numerical method of singular value decomposition, the six singular values of Jacobian matrix can be monitored. The sixth singular value for the Bricard linkage is always zero, which corresponds to the one degree of mobility. Meanwhile, there is some point that the fifth singular value becomes zero on the kinematic path, which is related to the bifurcation of the linkage.

Through numerical analysis, we are able to group the bifurcations into four cases, which will be discussed in detail next. By observing the bifurcated configurations, we are able to analytically derive the boundaries according to the ratio R/a and α. These boundaries are shown in Fig. 10.

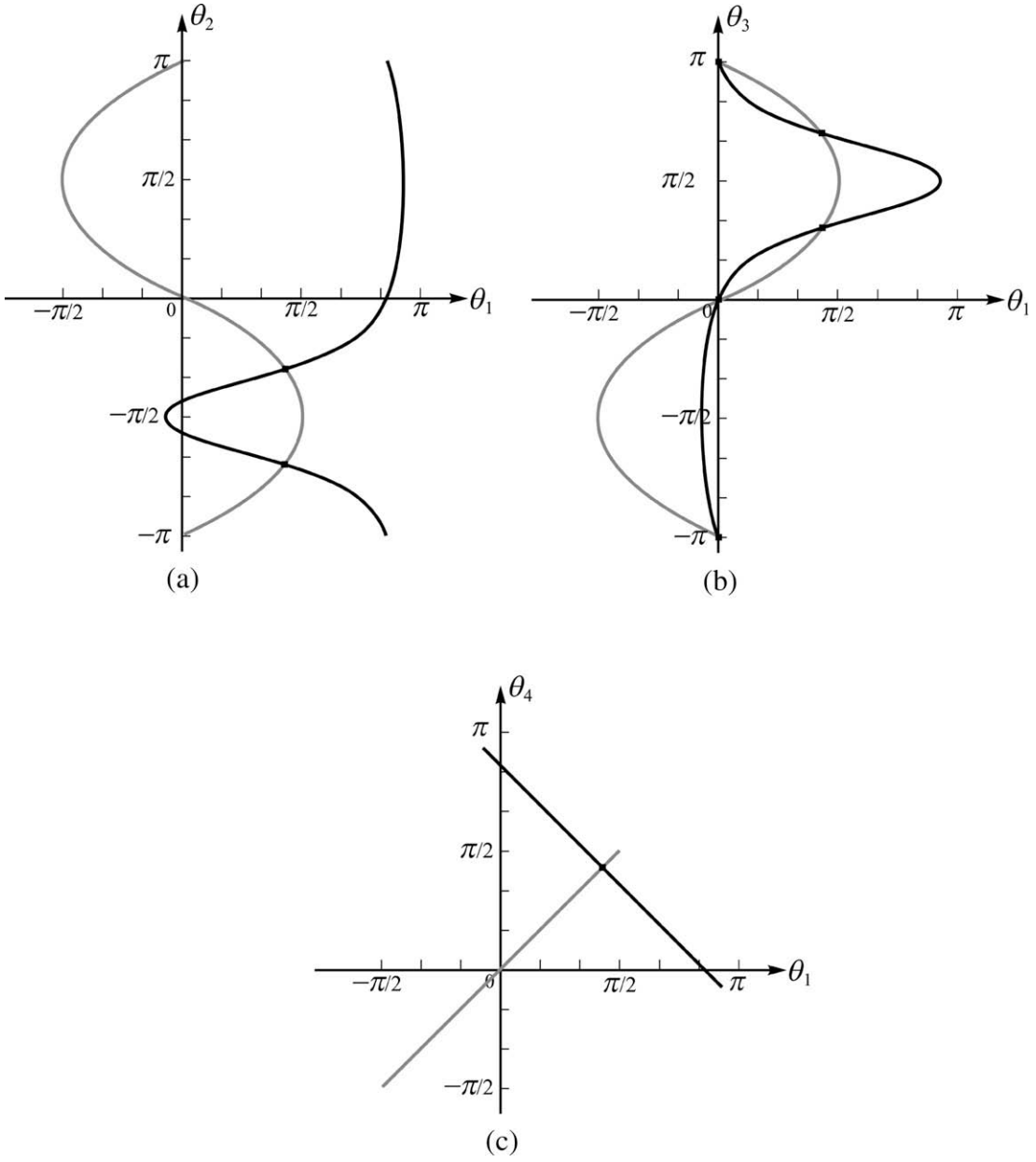

Fig. 16. The kinematic path of the linkage with $R/a = 4/5$ and $\alpha = \pi 2$. The path for the line and plane-symmetric Bricard linkage is in grey and the one for plane-symmetric Bricard linkage is in black. The intersection points of two paths in '■' are the bifurcation points. (a) θ_2 vs. θ_1; (b) θ_3 vs. θ_1; (c) θ_4 vs. θ_1, while $\theta_2 + \theta_6 = \pi,\ \theta_3 + \theta_5 = \pi$.

CASE I: $\frac{R}{a} > \cot\frac{\alpha}{2}\left(0 < \alpha \leqslant \frac{\pi}{2}\right)$ and $\frac{R}{a} \geqslant \tan\frac{\alpha}{2}\left(\frac{\pi}{2} < \alpha < \pi\right)$

A typical set of relationships between singular values and kinematic variable θ_1 is shown in Fig. 11 for a linkage with $R/a = 3/2$ and $\alpha = \pi/2$. The bifurcation occurs when $\theta_1^b = -67.38^\circ$. At this configuration the axes of hinges 2, 3, 5, and 6 meet at the same point due to the line and plane symmetry of the linkage. Such a configuration always exists on the kinematic path of a Case I linkage, as shown in Fig. 12. Considering the geometry, it can be found that at the bifurcation point,

$$\theta_1^b = -\arccos\frac{R^2 - a^2}{R^2 + a^2}. \tag{14g}$$

In fact, when bifurcation occurs the linkage becomes a 4*R* spherical linkage with revolute joints being 2, 3, 5, and 6. θ_1 and θ_4 do not change when the linkage moves to the new kinematic path after bifurcation, as shown in Fig. 13, implying that links 61 and 12 are rigidified into one link, so are the links 34 and 45. The motion sequence of this linkage passing the bifurcation point is shown in Fig. 14.

It can also been shown analytically using (10), (11) and (14) that θ_1^b is always between θ_1^d and θ_1^f.

Further study shows that this particular 4*R* spherical linkage also has bifurcation points also due to the symmetric geometry of the linkage. These bifurcations warrant in-depth investigation and they are not shown in Fig. 14.

CASE II: $\frac{R}{a} < \tan\frac{\alpha}{2}\left(0 < \alpha \leqslant \frac{\pi}{2}\right)$ and $\frac{R}{a} \leqslant \cot\frac{\alpha}{2}\left(\frac{\pi}{2} < \alpha < \pi\right)$

There is no such configuration as in Case I where the axes of revolute joints 2, 3, 5, and 6 meet at the same point. However, the fifth singular value still reaches zero when

$$\theta_1^b = \arccos\frac{a^2 - R^2}{a^2 + R^2}, \tag{14h}$$

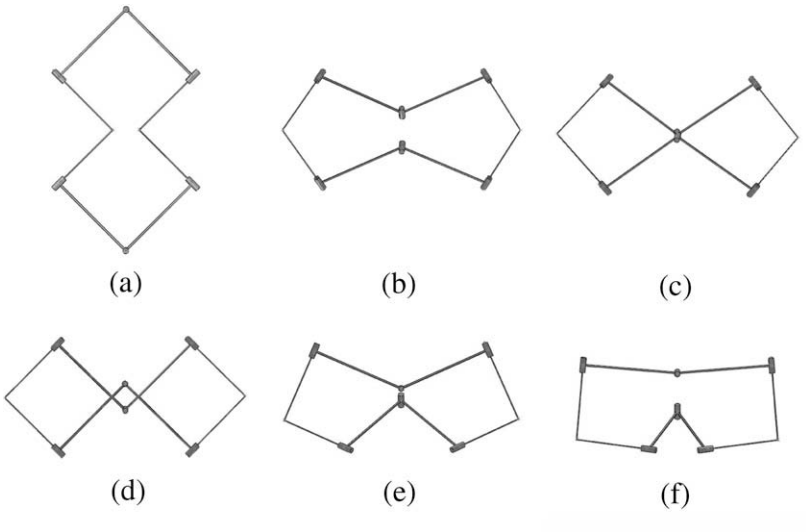

Fig. 17. Motion sequence of the linkage passing the bifurcation point. (a) Configuration with $\theta_1 = -\pi/2$ and $\theta_2 = \pi/2$; (c) bifurcation point; (b) and (d) on the path of line- and plane-symmetric Bricard linkage; (e) and (f) on the path of plane-symmetric Bricard linkage.

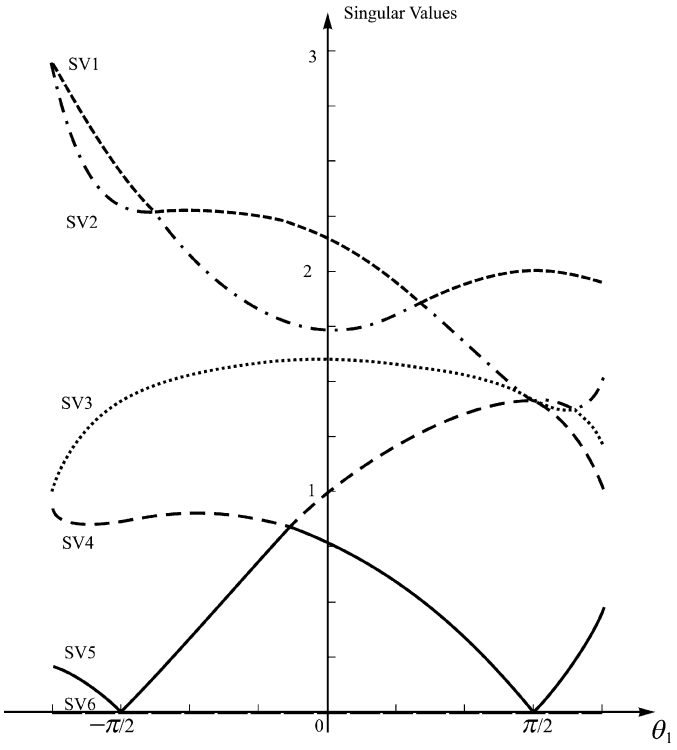

Fig. 18. Singular values of Jacobian matrix vs. θ_1 for a linkage with $R = a$ and $\alpha = \pi 3$. The sixth singular value (SV6) is always zero.

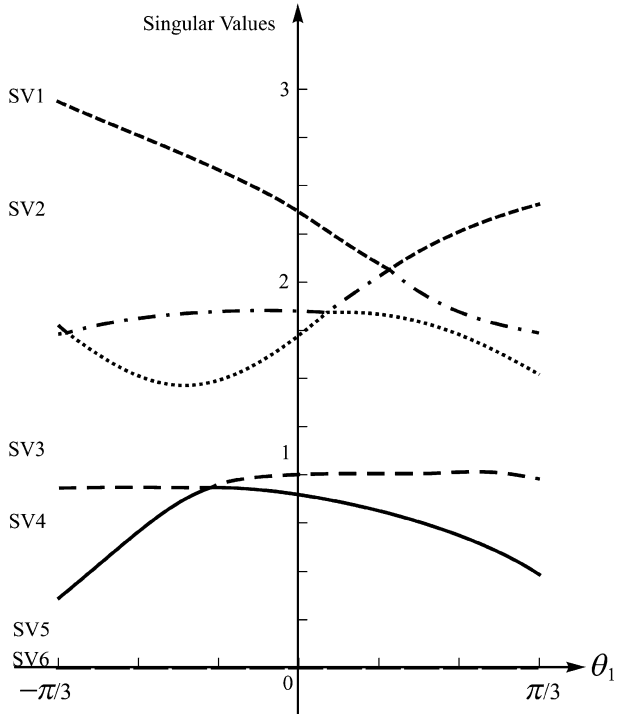

Fig. 19. Singular values of Jacobian matrix vs. θ_1 for the linkage with $R = a$ and $\alpha = 2\pi 3$. The sixth singular value (SV6) is always zero.

which is the configuration where revolute joints 1 and 4 are in the same position though the axes of the joints are not collinear. One example of the relationship between singular values and kinematic variable θ_1 is shown in Fig. 15, in which $R/a = 4/5$ and $\alpha = \pi/2$. The bifurcation happens when $\theta_1^b = 77.32^\circ$. The bifurcation leads the linkage into a kinematic path of a plane-symmetric Bricard linkage without line symmetry, see Fig. 16. The motion sequence of this linkage passing through the bifurcation point is shown in Fig. 17.

Similar to Case I, θ_1^b is always between θ_1^d and θ_1^f.

CASE III: $\tan\frac{\alpha}{2} \leqslant \frac{R}{a} \leqslant \cot\frac{\alpha}{2}\,(0 < \alpha \leqslant \frac{\pi}{2})$

In this case, the linkage has two bifurcation points. One is the bifurcation that transforms the linkage to a spherical 4*R* linkage, as in Case I, and the other to the plane-symmetric Bricard linkage as in Case II. For a linkage with $R/a = 1$ and $\alpha = \pi/3$ the relationship between singular values and kinematic variable θ_1 is shown in Fig. 18. And the kinematic paths are similar to the previous two cases.

CASE IV: $\cot\frac{\alpha}{2} < \frac{R}{a} < \tan\frac{\alpha}{2}\,(\frac{\pi}{2} < \alpha < \pi)$

In this case, the linkage does not have any bifurcation. A typical relationship between singular values and kinematic variable θ_1 is shown in Fig. 19 where $R/a = 1$ and $\alpha = 2\pi/3$.

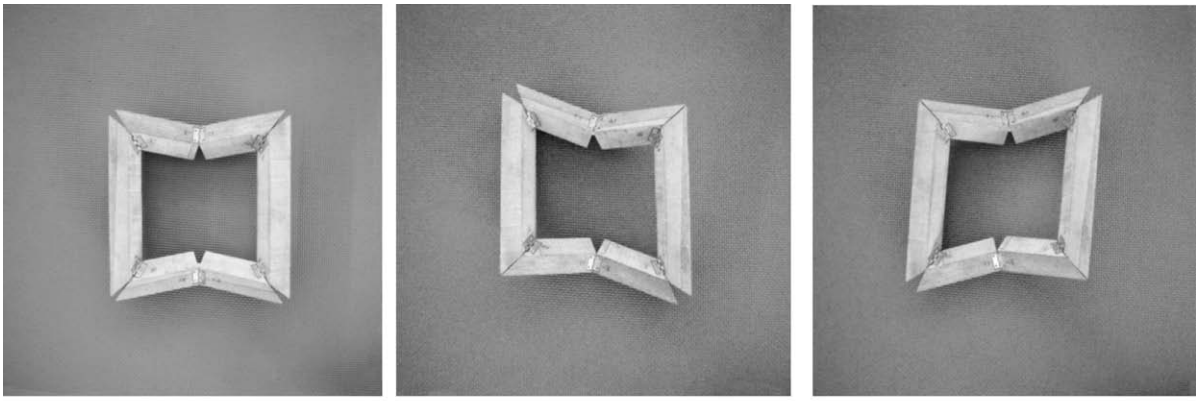

Fig. 20. The bifurcation of a model frame. (a) Bifurcation point; (b) and (c) two different configurations of the spherical 4R linkage in which the lower and upper middle hinges are frozen.

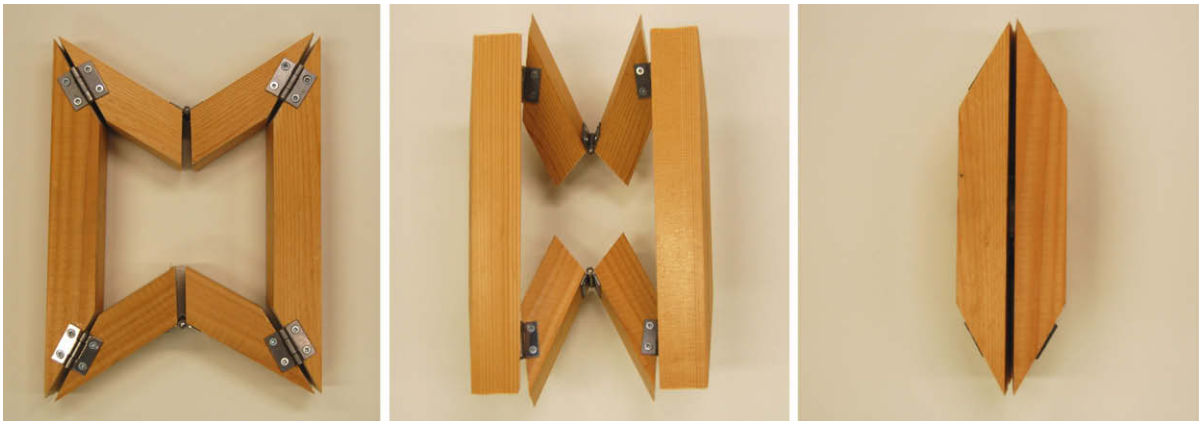

Fig. 21. The frame without bifurcation.

4. Design of frames without bifurcation

From the discussions above, Case IV frames do not have bifurcation. Hence, ideally the parameters that satisfy Case IV conditions should be used for the frame design. Prior to doing so, let us revisit the other conditions that a frame design should meet. First, the cutting angles between the horizontal and vertical links at the corners where they meet must be equal in order to have compact folding. For instance, in the case of the frame shown in Fig. 5, the corners are at joints 2, 3, 5 and 6 and the cutting angles is $\pi/4$ regardless what μ is. This is because the horizontal bars become parallel to the vertical ones when the frame is fully packaged. Secondly, the central revolute hinges always remain in the symmetrical plane, e.g., plane that passes joints 1 and 4 in the frame shown in Fig. 2. These requirements results in that α, the twists of the original Bricard linkage for those links corresponded to horizontal bars, can only be between 0 and $\pi/2$. Hence, for the 6*R* foldable frame shown in Fig. 5 with $2l_1 \leqslant l_2, 0 \leqslant \mu \leqslant \pi/2$, and, R/a is always greater than or equal to $\tan(\alpha/2)$ because of the geometric relationship given in (10) and (11). So this frame design always falls into Cases I or III with at least one bifurcation point at θ_1^b and $\theta_1^d \leqslant \theta_1^b \leqslant \theta_1^f$. The bifurcation of one of such frame models is shown in Fig. 20.

To use geometrical parameters which fall in the region of Case IV, we should aim for Bricard linkages with α greater than $\pi/2$. This only becomes possible when the horizontal bars are replaced by inclined bars. Fig. 21 shows such an example in which $R/a = 1$ and $\alpha = 2\pi/3$ ($\alpha_{12} = \alpha_{45} = 3\pi/2, \alpha_{23} = \alpha_{56} = \alpha = 2\pi/3$ and $\alpha_{34} = \alpha_{61} = \pi/2$). As expected no bifurcation is detected in the model. The design retains two-fold symmetry.

5. Conclusions and discussion

In this paper, we have identified the original linkage for the two-fold symmetrical 6*R* foldable frame proposed by Pellegrino et al. (2000) and Hutt (2007). It is in fact a line and plane-symmetric Bricard linkage. We have grouped the geometrical parameters of the linkage into four cases and using the singular value decomposition of the Jacobian matrix of closure equations, we have found bifurcations exist in its kinematic paths in three out of four cases. Moreover, the bifurcations exist between the folded and fully expanded configurations and therefore they are unavoidable in the proposed design.

Through our analysis, we show that only Case IV Bricard linkages do not have bifurcations. A frame design, which retains two-fold symmetry, is proposed. The appearance of this design differs from the previous one in that four horizontal bars are now inclined.

It should be noted that Hutt (2007) also suggested a bifurcation-free design which has only one-fold symmetry. In the design, the square section of the side members twists from one end to the other. Because our current study focuses on frames with two-fold symmetry, it is beyond the scope of this paper. However, the same

link could be made to the original Bricard linkages and its motion paths can be studied accordingly.

The bifurcations exist in current or any other frame designs may be utilised to build reconfigurable frames. This is a topic that warrants further investigation.

Acknowledgments

Y. Chen would like to acknowledge the support from the Nanyang Technological University, Singapore, in the form of a research Grant (RG21/05) and subsequent academic leave to undertake works related to this article. Z. You would like to thank Dalian University of Technology for awarding him a Haitian Fellowship during this research. Both authors are grateful to Mr. W. H. Chai and Mr. S.Y. Liu for the model fabrication and simulation in SolidWorks©, and to Mrs A. May for proofreading this paper.

Appendix A

Using the Denavit–Hartenberg notation (Beggs, 1966), the necessary and sufficient mobility condition for a closed loop linkage is shown in (12). For matrix $[T_{i(i+1)}]$, given in (13), the following relationship holds.

$$[T_{(i+1)i}] = [T_{i(i+1)}]^{-1} = \begin{bmatrix} C\theta_i & -C\alpha_{i(i+1)}S\theta_i & S\alpha_{i(i+1)}S\theta_i & a_{i(i+1)}C\theta_i \\ S\theta_i & C\alpha_{i(i+1)}C\theta_i & -S\alpha_{i(i+1)}C\theta_i & a_{i(i+1)}S\theta_i \\ 0 & -S\alpha_{i(i+1)} & C\alpha_{i(i+1)} & R_i \\ 0 & 0 & 0 & 1 \end{bmatrix}. \tag{A1}$$

In order to conduct the predictor and corrector step in the singular value decomposition of Jacobian matrix of the system as suggested by Gan and Pellegrino (2006), the transfer matrix in (13) is divide into two matrices, one is the transfer due to the link's geometric parameters, i.e., the two translations from link length $a_{i(i+1)}$ and the offset R_i, and the rotation from link twist $\alpha_{i(i+1)}$, marked as $[T^L_{i(i+1)}]$, which is constant for any configuration; the other is the transfer due to the rotation of revolute joint θ_i, marked as $[T^\theta_i]$, which is changed with the joint rotation. So we have

$$[T_{i(i+1)}] = [T^L_{i(i+1)}] \cdot [T^\theta_i] \tag{A2}$$

where

$$[T^L_{i(i+1)}] = \begin{bmatrix} 1 & 0 & 0 & -a_{i(i+1)} \\ 0 & C\alpha_{i(i+1)} & S\alpha_{i(i+1)} & -R_iS\alpha_{i(i+1)} \\ 0 & -S\alpha_{i(i+1)} & C\alpha_{i(i+1)} & -R_iC\alpha_{i(i+1)} \\ 0 & 0 & 0 & 1 \end{bmatrix}, \tag{A3a}$$

and

$$[T^\theta_i] = \begin{bmatrix} C\theta_i & S\theta_i & 0 & 0 \\ -S\theta_i & C\theta_i & 0 & 0 \\ 0 & 0 & 1 & 0 \\ 0 & 0 & 0 & 1 \end{bmatrix}. \tag{A3b}$$

The closure Eq. (12) then becomes

$$[T^L_{61}][T^\theta_6][T^L_{56}][T^\theta_5][T^L_{45}][T^\theta_4][T^L_{34}][T^\theta_3][T^L_{23}][T^\theta_2][T^L_{12}][T^\theta_1] = [I]. \tag{A4}$$

If taking revolute joint 1 as input of the linkage, see Fig. 6, the linkage moves from configurations θ_i to $\theta_i + \Delta\theta_i$ $(i = 1, 2, \ldots, 6)$. In both configurations, the closure Eq. (A4) should be satisfied. For a very small $\Delta\theta_i$, using the Taylor expansion of the kinematic variables and ignoring the higher-order terms, the transfer matrix of the revolute joint is

$$[T^{\theta+\Delta\theta}_i] = \begin{bmatrix} C(\theta_i+\Delta\theta_i) & S(\theta_i+\Delta\theta_i) & 0 & 0 \\ -S(\theta_i+\Delta\theta_i) & C(\theta_i+\Delta\theta_i) & 0 & 0 \\ 0 & 0 & 1 & 0 \\ 0 & 0 & 0 & 1 \end{bmatrix} \approx [T^\theta_i] + \begin{bmatrix} -S\theta_i & C\theta_i & 0 & 0 \\ -C\theta_i & -S\theta_i & 0 & 0 \\ 0 & 0 & 0 & 0 \\ 0 & 0 & 0 & 0 \end{bmatrix} \Delta\theta_i = [T^\theta_i] + [T^\theta_i]'\Delta\theta_i. \tag{A5}$$

Substituting (A5) into (A4) for each kinematic variable, we have

$$[T^L_{61}]\left([T^\theta_6] + [T^\theta_6]'\Delta\theta_6\right)[T^L_{56}]\left([T^\theta_5] + [T^\theta_5]'\Delta\theta_5\right)\cdots \times [T^L_{12}]\left([T^\theta_1] + [T^\theta_1]'\Delta\theta_1\right) = [I]. \tag{A6}$$

Or

$$\begin{aligned} &[T^L_{61}][T^\theta_6][T^L_{56}][T^\theta_5][T^L_{45}][T^\theta_4][T^L_{34}][T^\theta_3][T^L_{23}][T^\theta_2][T^L_{12}][T^\theta_1] \\ &+ \left([T^L_{61}][T^\theta_6]'[T^L_{56}][T^\theta_5][T^L_{45}][T^\theta_4][T^L_{34}][T^\theta_3][T^L_{23}][T^\theta_2][T^L_{12}][T^\theta_1]\right)\Delta\theta_6 \\ &+ \left([T^L_{61}][T^\theta_6][T^L_{56}][T^\theta_5]'[T^L_{45}][T^\theta_4][T^L_{34}][T^\theta_3][T^L_{23}][T^\theta_2][T^L_{12}][T^\theta_1]\right)\Delta\theta_5 \quad \cdots \\ &+ \left([T^L_{61}][T^\theta_6][T^L_{56}][T^\theta_5][T^L_{45}][T^\theta_4][T^L_{34}][T^\theta_3][T^L_{23}][T^\theta_2][T^L_{12}][T^\theta_1]'\right)\Delta\theta_1 = [I]. \end{aligned} \tag{A7}$$

Because of (A4), it can be derived that

$$[T_6]\Delta\theta_6 + [T_5]\Delta\theta_5 + \cdots + [T_1]\Delta\theta_1 = [0] \tag{A8}$$

where $[T_6] = [T^L_{61}][T^\theta_6]'[T^L_{56}][T^\theta_5][T^L_{45}][T^\theta_4][T^L_{34}][T^\theta_3][T^L_{23}][T^\theta_2][T^L_{12}][T^\theta_1], \ldots$, etc. $[T_i]$ $(i = 1, 2, \ldots, 6)$ has the following form

$$[T_i] = \begin{bmatrix} 0 & t_{i_{1,2}} & t_{i_{1,3}} & t_{i_{1,4}} \\ -t_{i_{1,2}} & 0 & t_{i_{2,3}} & t_{i_{2,4}} \\ -t_{i_{1,3}} & -t_{i_{2,3}} & 0 & t_{i_{3,4}} \\ 0 & 0 & 0 & 0 \end{bmatrix}$$

in which t's are non-zero elements in the matrix. Due to the skew-symmetry, $[T_i]$ has only six independent parameters which form the Plucker coordinates of each joint axis. Therefore, (A8) is equivalent to a 6×6 system of equations, whose coefficient matrix is known as the Jacobian of the system

$$\begin{bmatrix} T_{1_{1,2}} & T_{2_{1,2}} & T_{3_{1,2}} & T_{4_{1,2}} & T_{5_{1,2}} & T_{6_{1,2}} \\ T_{1_{1,3}} & T_{2_{1,3}} & T_{3_{1,3}} & T_{4_{1,3}} & T_{5_{1,3}} & T_{6_{1,3}} \\ T_{1_{2,3}} & T_{2_{2,3}} & T_{3_{2,3}} & T_{4_{2,3}} & T_{5_{2,3}} & T_{6_{2,3}} \\ T_{1_{1,4}} & T_{2_{1,4}} & T_{3_{1,4}} & T_{4_{1,4}} & T_{5_{1,4}} & T_{6_{1,4}} \\ T_{1_{2,4}} & T_{2_{2,4}} & T_{3_{2,4}} & T_{4_{2,4}} & T_{5_{2,4}} & T_{6_{2,4}} \\ T_{1_{3,4}} & T_{2_{3,4}} & T_{3_{3,4}} & T_{4_{3,4}} & T_{5_{3,4}} & T_{6_{3,4}} \end{bmatrix} \begin{bmatrix} \Delta\theta_1 \\ \Delta\theta_2 \\ \Delta\theta_3 \\ \Delta\theta_4 \\ \Delta\theta_5 \\ \Delta\theta_6 \end{bmatrix} = \begin{bmatrix} 0 \\ 0 \\ 0 \\ 0 \\ 0 \\ 0 \end{bmatrix}. \tag{A9}$$

When the system has one mobility, the large matrix on the left in (A9) will have a rank of 5 rather than full rank 6. This means that (A9) has a single set of infinity solutions and the six Plucker coordinates of the linkage are linearly dependent. So the solution of (A9) is the infinitesimal displacement of the linkage at the current configuration, which can be found by computing the singular value decomposition (SVD) of the Jacobian matrix.

In the numerical simulation, a small finite displacement, $\Delta\theta^p_i$ $(i = 1, 2, \ldots, 6)$, which is called predictor and proportional to the infinitesimal solution of (A9), is added to θ_i to update the linkage to the predicted configuration, $\theta^p_i = \theta_i + \Delta\theta^p_i$. However, this lin-

ear relationship is very likely to induce small errors to the kinematic paths, which is mostly non-linear. Therefore, under the predicted configuration, (A4) becomes

$$[T_{61}^{L}][T_{6}^{\theta p}][T_{56}^{L}][T_{5}^{\theta p}][T_{45}^{L}][T_{4}^{\theta p}][T_{34}^{L}][T_{3}^{\theta p}][T_{23}^{L}][T_{2}^{\theta p}][T_{12}^{L}][T_{1}^{\theta p}] = [I] + [E], \tag{A10}$$

where $[E]$ is the error matrix.

We therefore add a corrector, $\Delta\theta_i^c$, to the predictor displacement to make the linkage moves to the new correct configuration on the kinematic paths, i.e.

$$\theta_i^n = \theta_i^p + \Delta\theta_i^c = \theta_i + \Delta\theta_i^p + \Delta\theta_i^c, \tag{A11}$$

under which (A4) is satisfied.

$$[T_{61}^{L}][T_{6}^{\theta n}][T_{56}^{L}][T_{5}^{\theta n}][T_{45}^{L}][T_{4}^{\theta n}][T_{34}^{L}][T_{3}^{\theta n}][T_{23}^{L}][T_{2}^{\theta n}][T_{12}^{L}][T_{1}^{\theta n}] = [I]. \tag{A12}$$

From (A10)–(A12), it can be obtained that

$$[T_6^p]\Delta\theta_6^c + [T_5^p]\Delta\theta_5^c + \cdots + [T_1^p]\Delta\theta_1^c = [E] \tag{A13}$$

where $[T_6^p] = [T_{61}^{L}][T_6^{\theta p}]'[T_{56}^{L}][T_5^{\theta p}][T_{45}^{L}][T_4^{\theta p}][T_{34}^{L}][T_3^{\theta p}][T_{23}^{L}][T_2^{\theta p}][T_{12}^{L}][T_1^{\theta p}], \ldots,$ etc.

The solution of (A13) can be obtained with the same SVD method. The new configuration will be used as initial one for next iteration in calculation. And after a number of iterations, the full kinematic paths of the linkage can be found.

References

Baker, E.J., 1980. An analysis of Bricard linkages. Mechanism and Machine Theory 15, 267–286.

Beggs, J.S., 1966. Advanced Mechanism. Macmillan Company, New York.

Bricard, R., 1897. Mémoire sur la théorie de l'octaedre articulé. Journal de mathématiques pures et appliquées, Liouville 3, 113–148.

Bricard, R., 1927. Leçons de cinématique, Tome II Cinématique Appliquée. Gauthier-Villars, Paris. 7-12.

Chen, Y., 2003. Design of Structural Mechanisms. D. Phil. Dissertation. University of Oxford.

Chen, Y., You, Z., 2006. Square deployable frames for space applications: part I: theory. Proceedings of the IMechE 220 Part G: Journal of Aerospace Engineering 220, 347–354.

Crawford, R.F., Hedgepeth, J.M., Preiswerk, P.R., 1973. Spoked wheels to deploy large surfaces in space: weight estimates for solar arrays. NASA-CR-2347.

Cui, L., Dai, J.S., 2009. The axis constraint equation and a general 6R double-spherical overconstrained mechanism. In: Kecskeméthy, Andrés, Müller, Andreas (Eds.), Computational Kinematics. Springer-Verlag, Berlin, Heidelberg, pp. 233–240.

Fang, H., Lou, M., Huang, J., Quijano, U., Pelaez, G., 2004. Development of a 7-meter inflatable reflectarray antenna. AIAA paper 2004-1502, the 45th AIAA/ASME/ASCE/AHS/ASC Structures. Structural Dynamics & Materials Conference, Palm Springs. CA, USA.

Gan, W.W., Pellegrino, S., 2006. A numerical approach to the kinematic analysis of deployable structures forming a closed loop. Journal of Mechanical Engineering Science 220, 1045–1056.

Hutt, T., 2007. Deployable Rings. Fourth-year Undergraduate Project. University of Cambridge.

Lay, D.C., 2003. Linear Algebra and its Applications. Addison Wesley, 2003.

Pellegrino, S., Green, C., Guest, S.D., Watt, A., 2000. SAR advanced deployable structure. Technical Report. Department of Engineering, University of Cambridge.

Phillips, J., 1990. Freedom of Machinery, vol. 2. Cambridge University Press, Cambridge.